Supporting Information

Double-stranded metallo-triangles: from anion-templated nonanuclear to cation-templated tetraicosanuclear dysprosium clusters

Yanan Liu,[‡a] Xiao Sun,[‡a] Peiqiong Chen,[a] Xiaojuan Li,[a] Fu-Ping Huang,*[b] Hou-Ting Liu*[a] and Haiquan Tian*[a]

[a]Shandong Provincial Key Laboratory of Chemical Energy Storage and Novel Cell Technology, School of Chemistry and Chemical Engineering, Liaocheng University, Liaocheng 252059, P. R. China. E-mail: tianhaiquan@lcu.edu.cn; liuhouting@lcu.edu.cn

[b]Key Laboratory for the Chemistry and Molecular Engineering of Medicinal Resources (Ministry of Education of China), School of Chemistry and Pharmacy, Guangxi Normal University, Guilin, 541004, P. R. China. E-mail: huangfp2010@163.com

Table of Contents

Experimental Section

Synthesis

1-naphthylphosphonic acid ($C_{10}H_7PO_3H_2$) was prepared according to the methods reported in the literatures.[S1] All other reagents were purchased from commercial suppliers and as received without further purification. These two complexes were performed under aerobic conditions.

H_2L^1:

For (*E*)-*N'*-(3,5-di-*tert*-butyl-2-hydroxybenzylidene)pyrazine-2-carbohydrazide (**H_2L^1**): Pyrazine-2-carbohydrazide (10 mmol, 1.3812 g) was suspended together with 3,5-Di-*tert*-butyl-2-hydroxy-benzaldehyde (10 mmol, 2.3433 g) in methanol (40 ml), and the resulting mixture was stirred at the room temperature overnight. The pale yellow solid was collected by filtration (yield = 3.2031 g, 86%). Elemental analysis (%) calcd for $C_{20}H_{17}N_4O_2$: C, 69.55, H, 4.96, N, 16.22: found C, 68.06, H, 5.09, N, 15.65. IR (KBr, cm^{-1}): 3435(w), 3285(w), 2956(w), 1689(vs), 1651(w), 1585(m), 1524(s), 1467(w), 1437(m), 1398(w), 1357(w), 1309(m), 1269(w), 1251(m), 1236(m), 1209(m), 1157(w), 1107(m), 1052(m), 1022(s), 988(m), 963(w), 894(m), 860(m), 828(m), 770(m), 745(m), 672(m), 586(m), 446(m).

H_4L^2:

For ($N^{1'}E$,$N^{2'}E$)-$N^{1'}$,$N^{2'}$-bis(2-hydroxy-3-methoxybenzylidene)oxalohydrazide (**H_4L^2**): Oxalyl dihydrazide (10 mmol, 1.1811 g) was suspended together with *o*-vanillin (20 mmol, 3.0436 g) in methanol (100 ml), and the resulting mixture was stirred at the room temperature overnight. The pale yellow solid was collected by filtration (yield = 3.7598 g, 89%). Elemental analysis (%) calcd for $C_{18}H_{10}N_4O_6$: C, 57.15, H, 2.66, N, 14.81: found C, 55.92, H, 2.49, N, 15.06. IR (KBr, cm^{-1}): 3333(w), 3218(w), 2998(m), 2939(m), 2840(m), 1682(vs), 1605(s), 1577(w), 1517(vs), 1468(vs), 1359(s), 1256(vs), 1186(w), 1172(w), 1081(s), 1004(m), 967(w), 831(s), 782(w), 728(s), 570(m), 551(m), 507(w), 450(m).

Dy_9:

For $[Dy_9(L^1)_6(O_3PC_{10}H_7)_6(\mu_6\text{-}Cl)(SCN)_2(DMF)_6]\cdot 4DMF\cdot 5MeCN\cdot 1H_2O$ (**Dy_9**): A

mixture of H_2L^1 (34.53 mg, 0.10 mmol), $Dy(SCN)_3 \cdot 6H_2O$ (200.72 mg, 0.45 mmol) and NaN_3 (6.53 mg, 0.10 mmol) in H_2O/MeOH/MeCN/DMF (1:1:4:2, 24 mL) was heated with triethylamine (0.20 mL, 1.50 mmol) at 100 °C. After 4 h, $C_{10}H_7PO_3H_2$ (41.63 mg, 0.20 mmol) and NaCl (5.84 mg, 0.10 mmol) were added slowly to the solution. The resulting clear yellow-orange solution was sealed and kept in a vacuum drying oven at 100 °C. Dark-red block-like crystals were isolated after two weeks in 29% yield. Elemental analysis (%) calcd for $C_{222}H_{273}ClN_{41}Dy_9O_{41}P_6S_2$: C, 45.04; H, 4.65; N, 9.70; S, 1.08; Dy, 24.71; Na, 0.00; Cl, 0.60. Found: C, 43.59; H, 4.51; N, 9.48; S, 1.13; Dy, 25.94; Na, 0.00; Cl, 0.57. IR (KBr, cm^{-1}): 3423(w), 3051(m), 2954(w), 2064(w), 1660(vs), 1631(vs), 1614(vs), 1526(w), 1459(w), 1431(w), 1413(w), 1385(w), 1359(m), 1256(w), 1236(m), 1198(m), 1166(w), 1121(s), 1052(w), 1025(m), 1010(m), 963(m), 912(m), 912m(m), 861(m), 840(w), 801(m), 790(w), 775(w), 751(m), 676(w), 637(m), 584(w), 520(w), 486(w), 470(m), 449(m).

Dy_{24}:

For $[Dy_{24}Na_3(L^2)_6(O_3PC_{10}H_7)_6(\mu_4\text{-}O)_3(\mu_3\text{-}O)_{18}(\mu_2\text{-}AcO)_6(\mu_2\text{-}COO)_3(MeOH)_6(H_2O)_{18}]\cdot 20MeOH\cdot 90H_2O$ (**Dy_{24}**): A mixture of H_4L^2 (37.83 mg, 0.10 mmol) and $Dy(AcO)_3 \cdot 6H_2O$ (71.07 mg, 0.20 mmol) in H_2O/MeOH/DMF (1:4:1, 24 mL) was heated with solid NaOH (4.81 mg, 0.12 mmol) at 100 °C. After 10 h, $C_{10}H_7PO_3H_2$ (41.63 mg, 0.20 mmol) and $NaHCO_3$ (8.41 mg, 0.10 mmol) were added slowly to the solution. The resulting clear yellow-orange solution was sealed and kept in a vacuum drying oven at 100 °C. Pale-yellow block-like crystals were isolated after 6 days in 36% yield. Elemental analysis (%) calcd for $C_{209}H_{473}Dy_{24}N_{24}Na_3O_{227}P_6$: C, 22.59; H, 4.29; N, 3.03; Dy, 35.10; Na, 0.62; Cl, 0.00. Found: C, 21.68; H, 4.43; N, 2.91; Dy, 35.64; Na, 0.59; Cl, 0.00. IR (KBr, cm^{-1}): 3422(w), 2934(m), 1663(vs), 1601(vs), 1469(vs), 1363(s), 1237(w), 1214(s), 1168(m), 1082(s), 1010(w), 967(w), 869(w), 829(m), 801(m), 780(w), 743(s), 664(w), 649(m), 636(m), 623(m), 564(w), 546(m), 518(m), 501(m).

Analytical Procedures

General methods: Elemental analyses were carried out in a $PE_{240}C$ elemental analyzer. The infrared spectra were recored as KBr pellets on a Bruker Tensor 27

spectrometer in the range of 400-4000 cm^{-1}. Thermal analyses were performed on a METTLER TOLEDO TGA/DSC 1 instrument in the range of 30-800 °C with Al_2O_3 pan at a heating rate of 5 ºC/min. Powder X-ray diffraction data were collected using a Bruker D8 ADVANCE PXRD equipped with a CuKα X-ray source over the 2θ range of 5 to 50° at room temperature. Energy-dispersive X-ray spectra were recorded with the help of a HRTEM, Thermo Fischer, Talos F200x. The magnetic susceptibility data were obtained on a Quantum Design MPMS3 SQUID system. The direct current measurements were obtained with an external magnetic field of 1.0 kOe in the temperature range 1.8-300 K, and the alternating-current measurements were executed in a 3.0 Oe *ac* oscillating field at different frequencies from 1 to 1000 Hz. The diamagnetic contribution of the sample itself was estimated from Pascal's constant.[S2]

Crystal structure determination and refinement: All crystals were taken from the mother liquid without further treatment, transferred to oil and mounted into a loop for single crystal X-ray data collection. Diffraction intensity data of **Dy_9** was collected on a ROD, XtaLAB Synergy Custom DW system, HyPix diffractometer using Cu Kα (λ = 1.54184 Å) at 100 K, whereas that of **Dy_{24}** on a multiwire proportional diffractometer using graphite-monochromated Mo Kα (λ = 0.71073 Å) at 100 K. The diffraction images were processed using the *CrystAlis^{Pro}* software suite.[S3] These structures were solved using the charging-flipping algorithm, as implemented in the program *SUPERFLIP*[S4] and refined by full-matrix least-squares techniques against F_o^2 using the SHELXL program[S5] through the OLEX2 interface.[S6] Hydrogen atoms were placed in calculated positions and refined isotropically by using a riding model. All structures were examined using the Addsym subroutine of PLATON[S7] to ensure that no additional symmetry could be applied to the models. Nevertheless, in this heavy-atom structure as it was not possible to see clear electron-density peaks in difference maps which would correspond with acceptable locations for the various H atoms bonded to water oxygen atoms, the refinement was completed with no allowance for these H atoms in the model.

There are some solvent-accessible void volumes in the crystals of **Dy_9** and **Dy_{24}**,

which are occupied by highly disordered water and manthanol molecules. No satisfactory disorder model could be achieved despite numerous attempts, and therefore the SQUEEZE program[S8] implemented in PLATON was further employed to remove these electron densities. For **Dy_9**, the SQUEEZE function of PLATON reveals a residual electron density of 288 electrons/cell in cell-remaining voids where the residual electron density was tentatively assigned to 4 dimethylformamide molecules, 5 acetonitrile molecules and 1 water molecules [288 = 4 (DMF) × 40*e* + 22 (MeCN) × 22*e* + 1 (H_2O) × 10*e*]. For **Dy_{24}**, the SQUEEZE function of PLATON reveals a residual electron density of 1260 electrons/cell in cell-remaining voids where the residual electron density was tentatively assigned to 20 methanol molecules and 90 water molecules [1260 = 20 (MeOH) × 18*e* + 90 (H_2O) × 10*e*]. The amount of lattice solvent molecules was proved by TG analysis (please see Figure S2). The reported sum formula has been corrected by taking into account the lattice methanol and water molecules. Pertinent crystallographic data collection and refinement parameters are collated in Table S1.

CCDC 2253521 (**Dy_9**) and CCDC 2253522 (**Dy24**) contain the supplementary crystallographic data for this paper. These data can be obtained free of charge from the Cambridge Crystallographic Data Centre via www.ccdc.cam.ac.uk/data_request/cif.

Structure information

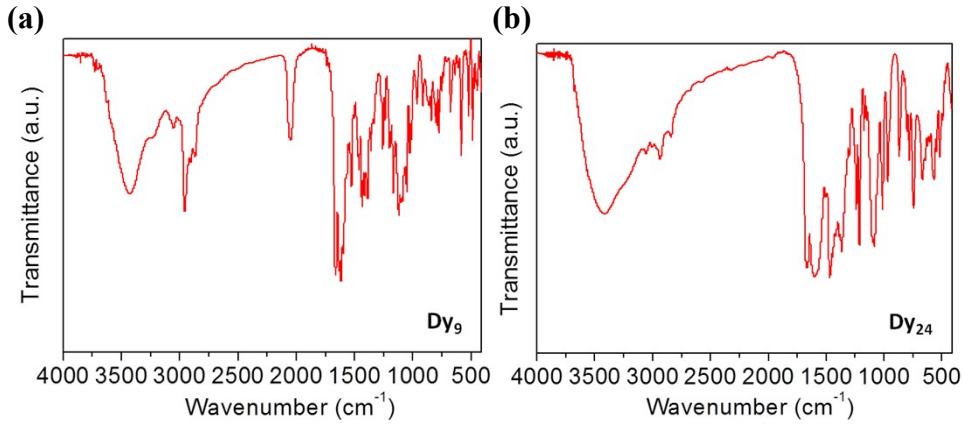

Figure S1. Infrared spectra of **Dy$_9$** (a) and **Dy$_{24}$** (b).

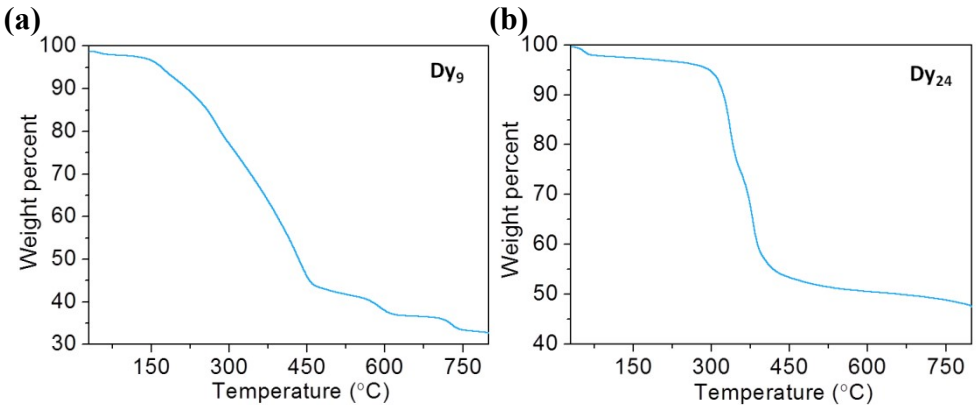

Figure S2. Thermal analysis of **Dy$_9$** (a) and **Dy$_{24}$** (b).

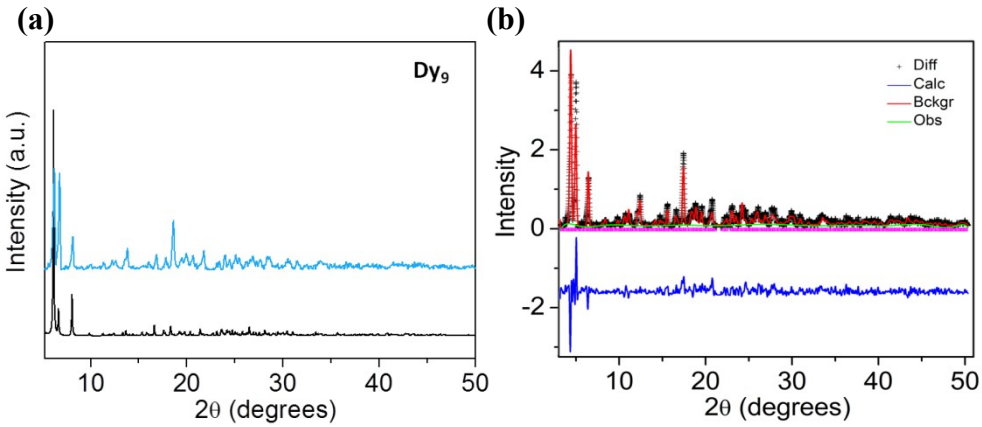

Figure S3. The powder XRD patterns for **Dy$_9$** (a). The black circles are for the observed data (b). The red solid line is for the calculated data. The grey solid curve is for the difference. The vertical bars are the positions of Bragg peaks. Cell parameters: *R*-3*c*, a = 23.84 Å, b = 23.84 Å, c = 78.24 Å, α = 90.0°, β = 90.0°, γ = 120.0°, V = 39016.1 Å^3 (wRp = 0.109).

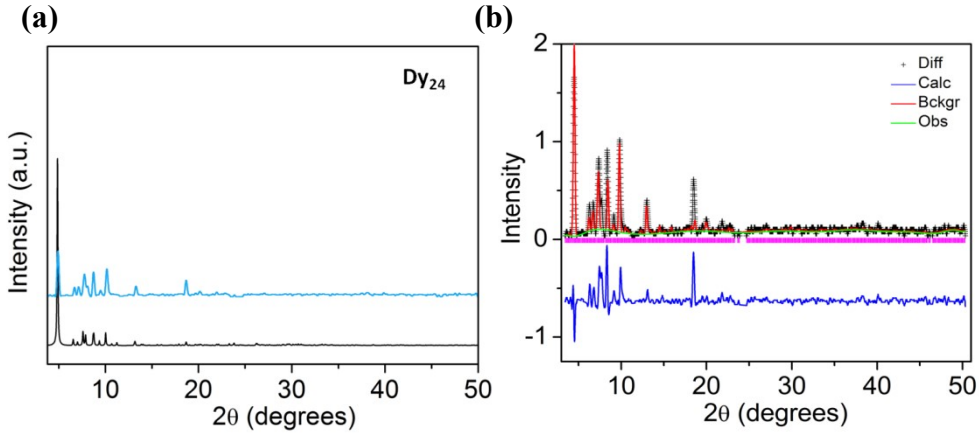

Figure S4. The powder XRD patterns for **Dy$_{24}$** (a). The black circles are for the observed data (b). The red solid line is for the calculated data. The grey solid curve is for the difference. The vertical bars are the positions of Bragg peaks. Cell parameters: *R*-3*c*, a = 40.01 Å, b = 40.01 Å, c = 41.95 Å, α = 90.0°, β = 90.0°, γ = 120.0°, V = 59122.9 Å^3 (wRp = 0.116).

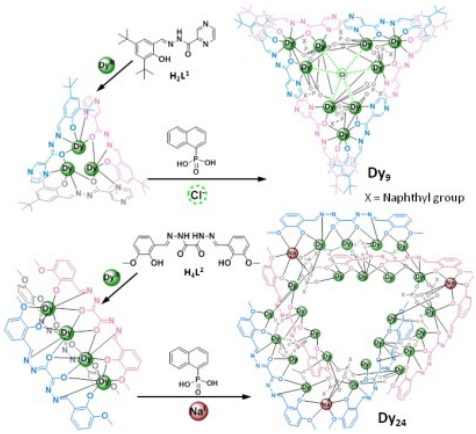

Scheme S1. Preparation of compounds **Dy$_9$** (a) and **Dy$_{24}$** (b).

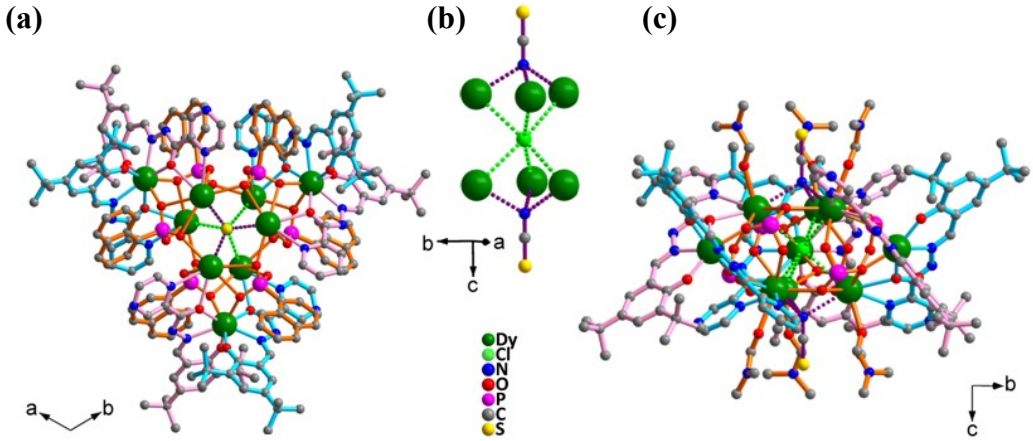

Figure S5. Ball-and-stick views of **Dy$_9$**. View along the crystallographic *c* axis (a). The $[Dy_6(\mu_6\text{-}Cl)(\mu_3\text{-}N_3)_2]^{15+}$ core (b). View along the crystallographic *a* axis (c). The hydrogen atoms are omitted for clarity.

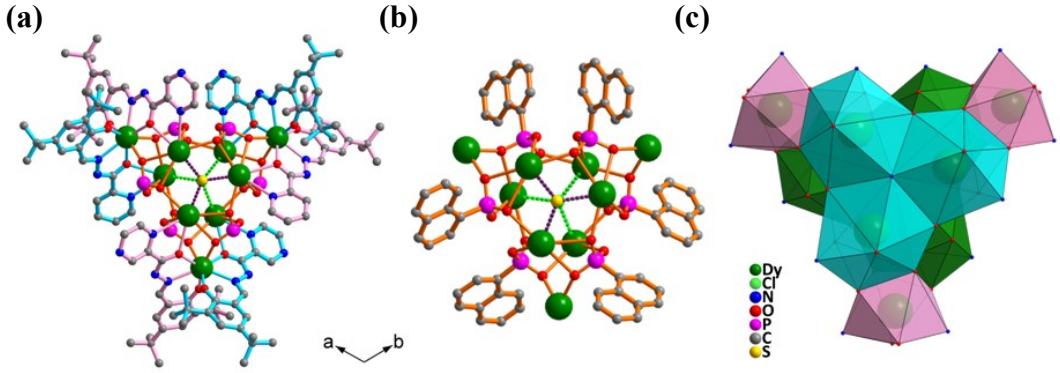

Figure S6. Structure **Dy$_9$** highlighting the coordination modes of $(L^2)^{4-}$ (a) and $C_{10}H_7PO_3^{2-}$ (b). Coordination polyhedra observed for the metal centers (c).

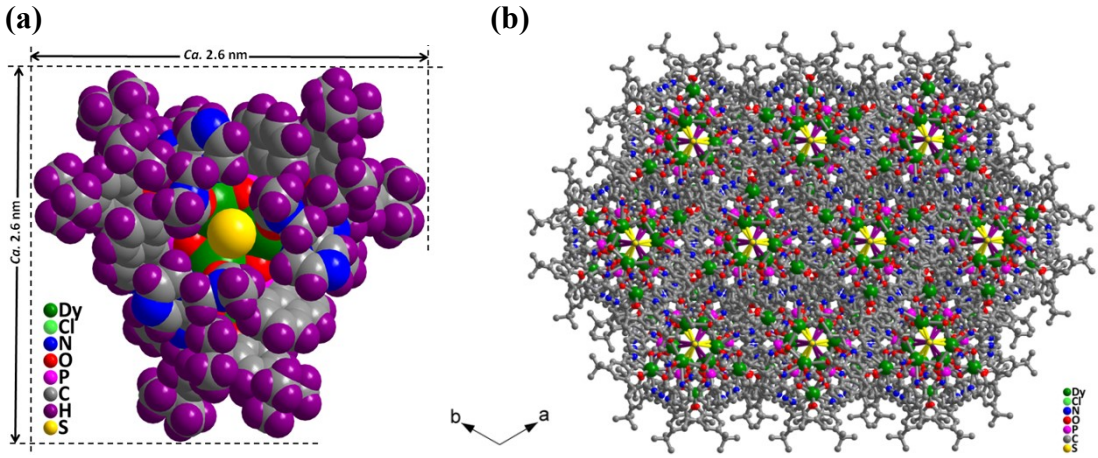

Figure S7. Space-filling representation of **Dy$_9$** (a). The molecular packing viewed along the *c* axis (b).

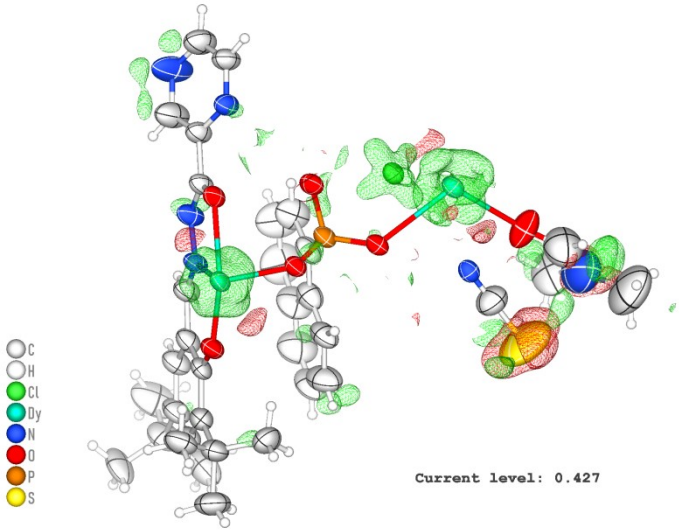

Figure S8. Residual density map of **Dy$_9$**.

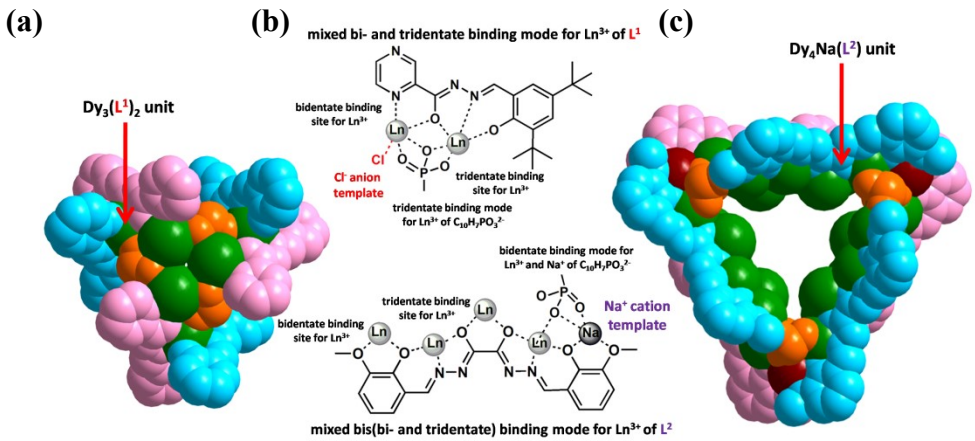

Figure S9. Space filling representation of the $[Dy_3(L^1)_2(O_3P)_2]_3^{3+}$ (a) and the $[Dy_4Na(L^2)(O_3P)]_6^{7+}$ (c) units (the tertiary butyl and the naphthyl groups, encapsulated ions of chloride, formate and acetate as well as the coordinating water, methanol and DMF molecules are omitted); representation of the different binding modes of L^1 and L^2 ligands, and $C_{10}H_7PO_3^{2-}$ co-ligand, and Cl^- anion (b).

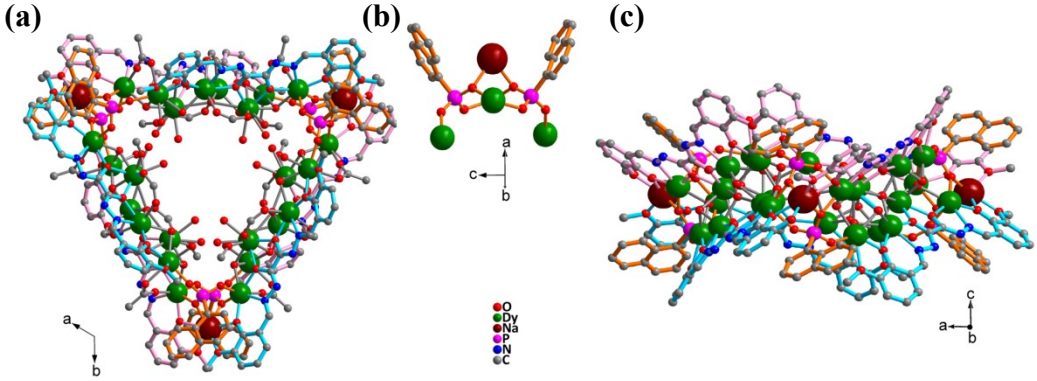

Figure S10. Ball-and-stick views of **Dy_{24}**. View along the crystallographic *c* axis (a). The $[Dy_4Na(O_3PC_{10}H_7)_2]^{9+}$ core (b). View along the crystallographic *a* axis (c). Hydrogen atoms are omitted for clarity.

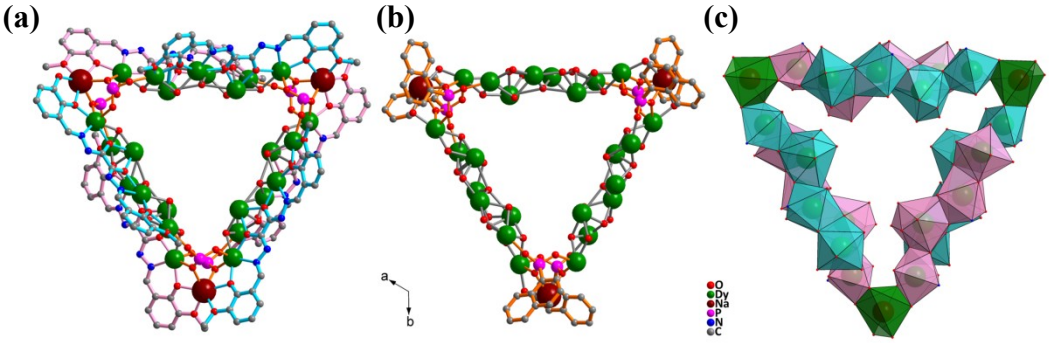

Figure S11. Structure **Dy_{24}** highlighting the coordination modes of $(L^2)^{4-}$ (a) and $C_{10}H_7PO_3^{2-}$ (b). Coordination polyhedra observed for the metal centers (c).

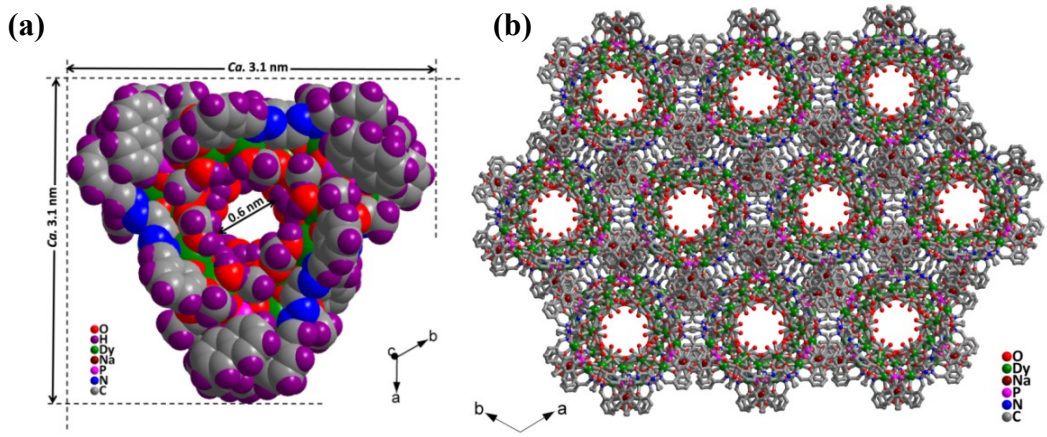

Figure S12. Space-filling representation of **Dy$_{24}$** (a). The molecular packing viewed along the *c* axis (b).

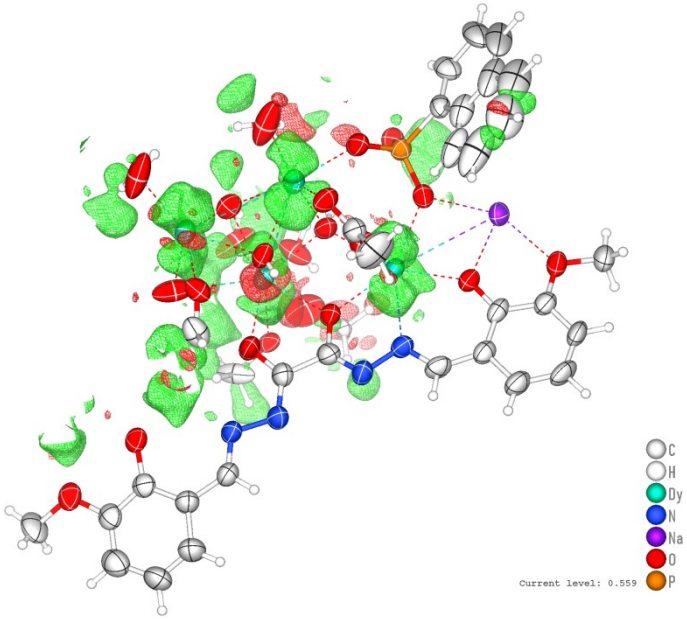

Figure S13. Residual density map of **Dy$_{24}$**.

Table S1. Summary of structural data of **Dy_9** and **Dy_{24}**.

	Dy_9	**Dy_{24}**
CCDC number	2253521	2253522
Formula	$C_{222}H_{273}ClN_{41}Dy_9O_{41}P_6S_2$	$C_{209}H_{473}Dy_{24}N_{24}Na_3O_{227}P_6$
Formula weight	5919.72	11109.83
Crystal size (mm^3)	0.09 × 0.08 × 0.08	0.16 × 0.16 × 0.12
Temperature (K)	100.00(10)	100(2)
Crystal system	Trigonal	Trigonal
Space group	*R*-3*c* #167	*R*-3*c* #167
a (Å)	24.09003(14)	40.2966(4)
b (Å)	24.09003(14)	40.2966(4)
c (Å)	79.8295(6)	42.4712(5)
α (°)	90	90
β (°)	90	90
γ (°)	120	120
Volume ($Å^3$)	40120.7(6)	59725.8(14)
Z	6	6
ρ_{calcd} (g/cm^3)	1.470	1.476
2θ (deg)	2.378 to 74.970	1.617 to 30.892
F(000)	16038	24948
Reflns collected	84053	124818
Unique reflns	8000	11735
R_{int}	0.084	0.036
GOOF	0.765	0.760
$R1^a$	0.0526	0.0447
$wR2^b$	0.1699	0.1710

Table S2. Selected bond lengths (Å) and angles (º) for **Dy$_9$**.

Dy$_9$					
Dy1-O1	2.307(3)	Dy1-O4	2.488(4)	Dy1-O5	2.215(4)
Dy1-N3	2.535(5)	Dy1 -O1d	2.307(4)	Dy1-O4d	2.488(5)
Dy1-O5d	2.215(5)	Dy1-N3d	2.535(6)	Dy2-O3	2.701(3)
Dy2-O6	2.656(6)	Dy2-O2e	2.811(6)	Dy2-O4e	2.813(4)
S1-C36	1.632(17)	P1-O2	1.553(4)	P1-O3	1.517(4)
P1-O1	1.513(4)	P1-C1	1.799(8)	O4-C16	1.239(9)
O5-C23	1.298(9)	O6-C34	1.216(15)	N1-C12	1.323(14)
N1-C14	1.331(15)	N2-N3	1.405(7)	N2-C16	1.331(9)
N3-C17	1.291(9)	N4-C32	1.51(3)	N4-C33	1.54(3)
N4-C34	1.40(2)	N6-C15	1.331(9)	N6-C11	1.318(8)
N5-C36	1.121(17)	O1-Dy1-O4	78.49(12)	O3-Dy2-O6	108.3(2)
O1-Dy1-O5	94.59(13)	O2e-Dy2-O3	72.66(12)	O1-Dy1-N3	84.44(15)
O3-Dy2-O4e	120.18(13)	O1-Dy1-O1d	80.90(14)	O2e-Dy2-O6	137.1(2)
O1-Dy1-O4d	68.72(14)	O4e-Dy2-O6	83.2(2)	O1-Dy1-O5d	156.06(18)
O2e-Dy2-O4e	62.47(13)	O1-Dy1-N3d	131.40(16)	O1-P1-O2	108.3(2)
O4-Dy1-O5	133.70(17)	O1-P1-O3	108.3(2)	O4-Dy1-N3	62.97(15)
O1-P1-C1	109.6(3)	O1d-Dy1-O4	68.73(15)	O2-P1-O3	110.9(2)
O4-Dy1-O4d	136.62(14)	O2-P1-C1	105.1(3)	O4-Dy1-O5d	77.99(17)
O3-P1-C1	112.0(3)	O4-Dy1-N3d	136.76(14)	Dy1-O1-P1	144.9(2)
O5-Dy1-N3	70.83(17)	O1d-Dy1-O5	156.06(16)	O4d-Dy1-O5	77.99(16)
O5-Dy1-O5d	98.42(17)	O5-Dy1-N3d	81.00(17)	O1d-Dy1-N3	131.38(15)
O4d-Dy1-N3	136.75(15)	O5d-Dy1-N3	81.01(19)	N3-Dy1-N3d	136.45(17)
O1d-Dy1-O4d	78.48(14)	O1d-Dy1-O5d	94.61(17)	O1d-Dy1-N3d	84.47(17)
O4d-Dy1-O5d	133.72(18)	O4d-Dy1-N3d	63.00(16)	O5d-Dy1-N3d	70.8(2)

Symmetry codes: a: 1 - *y*, *x* - *y*, *z*; b: 1- *x* + *y*, 1- *x*, *z*; c: 1/3 + *y*, -1/3 + *x*, 7/6 - *z*; d: 4/3 - *x*, 2/3 -*x* + *y*, 7/6 - *z*; e: 1/3 + *x* - *y*, 2/3 - *y*, 7/6 - *z*.

Table S3. Selected bond lengths (Å) and angles (º) for **Dy_{24}**.

Dy_{24}					
Dy1-O7	2.324(8)	Dy1-O8	2.369(5)	Dy1-O9	2.353(13)
Dy1-O10	2.376(7)	Dy1-O13	2.379(6)	Dy1-O2e	2.295(6)
Dy1-O3e	2.319(6)	Dy1-N1e	2.521(10)	Dy2-O3	2.344(8)
Dy2-O4	2.367(7)	Dy2-O8	2.815(2)	Dy2-O10	2.435(6)
Dy2-O12	2.351(6)	Dy2-O13	2.352(7)	Dy2-O29	2.362(19)
Dy2-O30	2.387(14)	Dy2-O29'	2.32(2)	Dy2-O30'	2.299(13)
Dy3-O4	2.310(6)	Dy3-O5	2.245(6)	Dy3-O12	2.425(7)
Dy3-O16	2.299(6)	Dy3-O18	2.252(8)	Dy3-N4	2.505(8)
Dy3-O15d	2.271(7)	Dy4-O10	2.418(7)	Dy4-O12	2.384(6)
Dy4-O13	2.363(6)	Dy4-O14	2.226(6)	Dy4-O17	2.381(9)
Dy4-O19	2.362(13)	Dy4-O1e	2.502(7)	Dy4-O2e	2.375(6)
P1-O14	1.518(7)	P1-O15	1.536(8)	P1-O16	1.522(6)
P1-C19	1.823(7)	Na1-O5	2.412(7)	Na1-O6	2.349(7)
Na1-O16	2.362(6)	Na1-O5d	2.412(7)	Na1-O6d	2.348(7)
Na1-O16d	2.362(7)	O1-C1	1.447(13)	O1-C2	1.397(14)
O2-C3	1.363(11)	O3-C9	1.313(13)	O4-C10	1.332(14)
O5-C17	1.297(13)	O6-C16	1.389(14)	O6-C18	1.454(12)
O7-C30	1.244(10)	O9-C33'e	1.29(3)	O17-C31	1.220(12)
O18-C31	1.260(14)	O30-C33	1.332(17)	Dy1-O8-Dy2	89.33(6)
Dy1-O8-Dy1e	131.9(5)	Dy1-O8-Dy2e	98.18(7)	Dy1e-O8-Dy2	98.17(7)
Dy1-O10-Dy2	99.0(3)	Dy1-O10-Dy4	95.6(3)	Dy2-O10-Dy4	94.5(2)
Dy1e-O3-Dy2	114.8(3)	Dy2-O4-Dy3	114.7(3)	Dy3-O5-Na1	99.2(3)
Dy2-O12-Dy3	111.1(3)	Dy2-O12-Dy4	97.7(2)	Dy3-O12-Dy4	114.1(3)
Dy1-O13-Dy2	97.0(2)	Dy1-O13-Dy4	98.2(3)	Dy2-O13-Dy4	98.2(3)
Dy3-O16-Na1	99.2(2)				

Symmetry codes: a: 1 - *y*, *x* - *y*, *z*; b: 1 - *x* + *y*, 1 - *x*, *z*; c: 1/3 + *y*, -1/3 + *x*, 7/6 - *z*; d: 4/3 - *x*, 2/3 - *x* + *y*, 7/6 - *z*; e: 1/3 + *x* - *y*, 2/3 - *y*, 7/6 - *z*.

Table S4. Dy^{III} geometry analysis of **Dy_9** and **Dy_{24}** by SHAPE 2.1 software.

Dy_9

Geometry (CN = 8)	Dy1	Geometry (CN = 9)	Dy2
OP-8	30.561	**EP-9**	29.982
HPY-8	25.443	**OPY-9**	21.513
HBPY-8	14.585	**HBPY-9**	16.156
CU-8	12.425	**JTC-9**	14.342
SAPR-8	4.273	**JCCU-9**	9.380
TDD-8	2.224	**CCU-9**	7.410
JGBF-8	9.582	**JCSAPR-9**	7.180
JETBPY-8	24.551	**CSAPR-9**	5.570
JBTPR-8	3.098	**JTCTPR-9**	7.750
BTPR-8	2.801	**TCTPR-9**	6.020
JSD-8	1.788	**JTDIC-9**	12.828
TT-8	13.240	**HH-9**	6.001
ETBPY-8	21.118	**MFF-9**	4.354

Dy_{24}

Geometry (CN = 8)	Dy1	Dy2	Dy4	Geometry (CN = 7)	Dy3	Geometry (CN = 6)	Na1
OP-8	29.383	32.690	29.338	**HP-7**	32.606	**HP-6**	21.560
HPY-8	23.995	20.301	23.707	**HPY-7**	22.612	**PPY-6**	10.093
HBPY-8	13.331	16.426	15.562	**PBPY-7**	1.216	**OC-6**	13.627
CU-8	10.370	14.492	12.295	**COC-7**	5.498	**TPR-6**	9.769
SAPR-8	2.274	5.182	2.783	**CTPR-7**	4.239	**JPPY-6**	12.552
TDD-8	1.602	3.370	1.329	**JPBPY-7**	4.073		
JGBF-8	11.703	12.986	12.979	**JETPY-7**	22.802		
JETBPY-8	27.708	26.397	27.556				
JBTPR-8	2.618	3.666	2.558				
BTPR-8	1.812	2.128	1.920				
JSD-8	2.728	5.158	3.367				
TT-8	10.852	14.998	13.040				
ETBPY-8	24.757	21.008	23.780				

Magnetic properties of Dy_9 and Dy_{24}

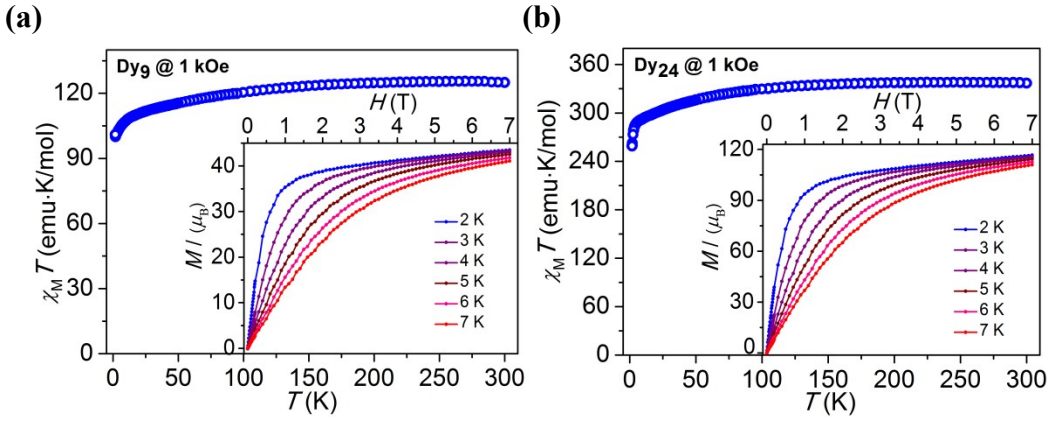

Figure S14. Temperature dependent of the $\chi_M T$ values at 1.0 kOe for compounds **Dy_9** (a) and **Dy_{24}** (b). Inset: the magnetization *vs.* field plots at different temperature.

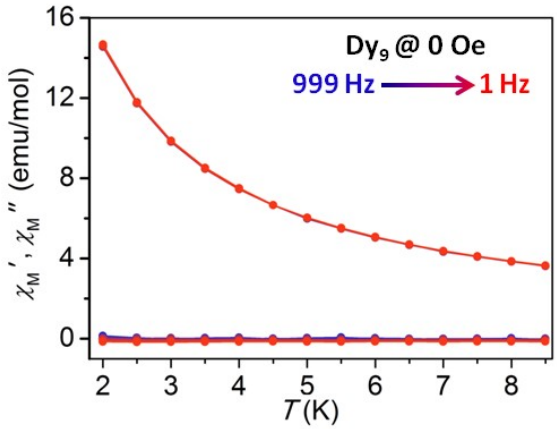

Figure S15. Temperature dependence of χ_M' and χ_M'' in zero dc field for **Dy_9**.

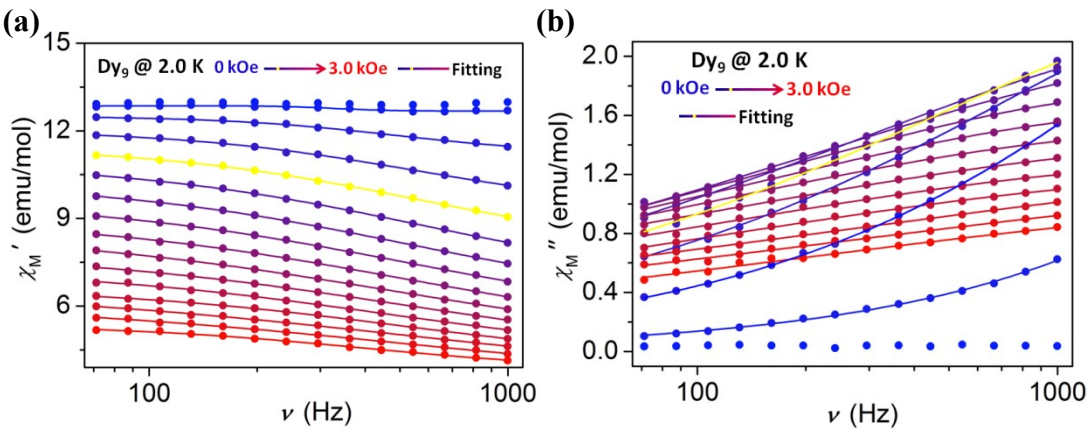

Figure S16. Frequency and field dependence of χ_M' (a) and χ_M'' (b) at 2.0 K for **Dy_9**. The solid lines are the best fits to the experimental data, obtained with the generalized Debye model.

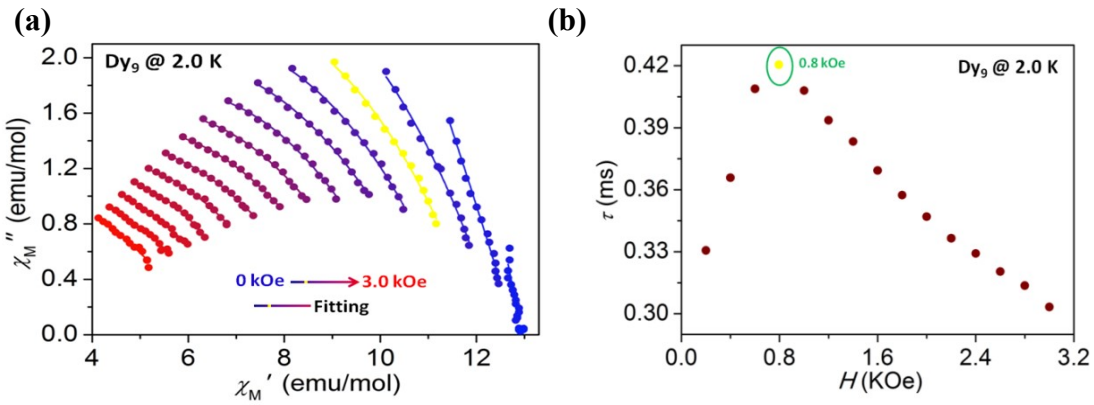

Figure S17. Cole-Cole plots at 2.0 K between 0 and 3.0 kOe for **Dy$_9$** (a). The solid lines are the best fits to the experimental data, obtained with the generalized Debye model. Magnetization relaxation time, *τ versus H* plots (b).

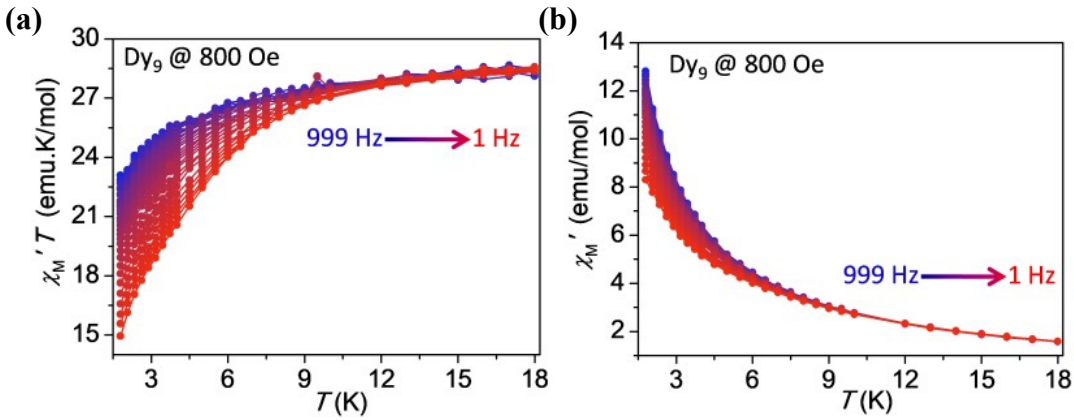

Figure S18. Temperature dependence of the $\chi_M'T$ (a) and χ_M' (b) in a 800 Oe dc field for **Dy$_9$**.

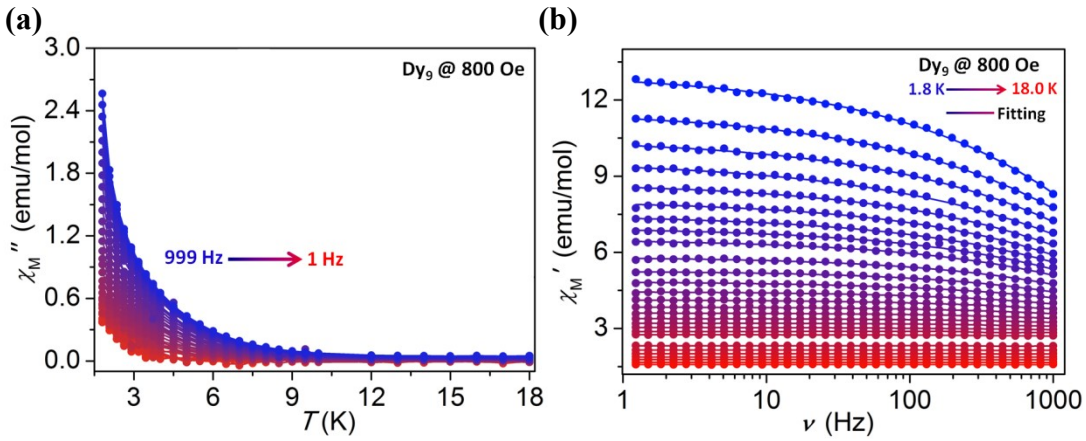

Figure S19. Temperature dependence of χ_M'' (a) and frequency dependence of χ_M' (b) in a 800 Oe dc field for **Dy$_9$**.

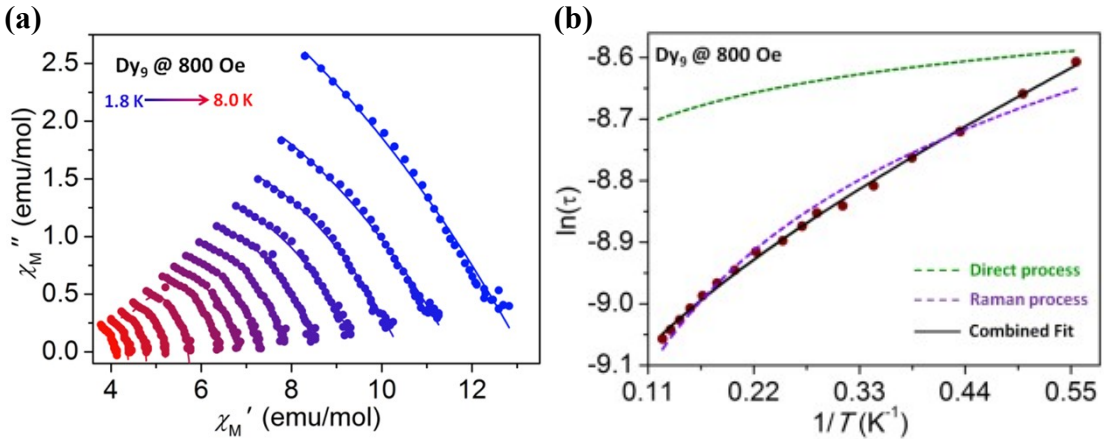

Figure S20. Cole-Cole plots for compound **Dy$_9$** collected under a 800 Oe dc magnetic field. Data were collected at the temperature of 1.8 K and 8.0 K (a). The solid lines represent fits to the data using the generalized Debye model. Plots of ln(τ) *vs.* 1/*T*: magnetization relaxation times extracted from ac susceptibility measurements (b). Black lines represent overall fits to the data. Green and violet lines represent the direct and Raman components of the fit, respectively.

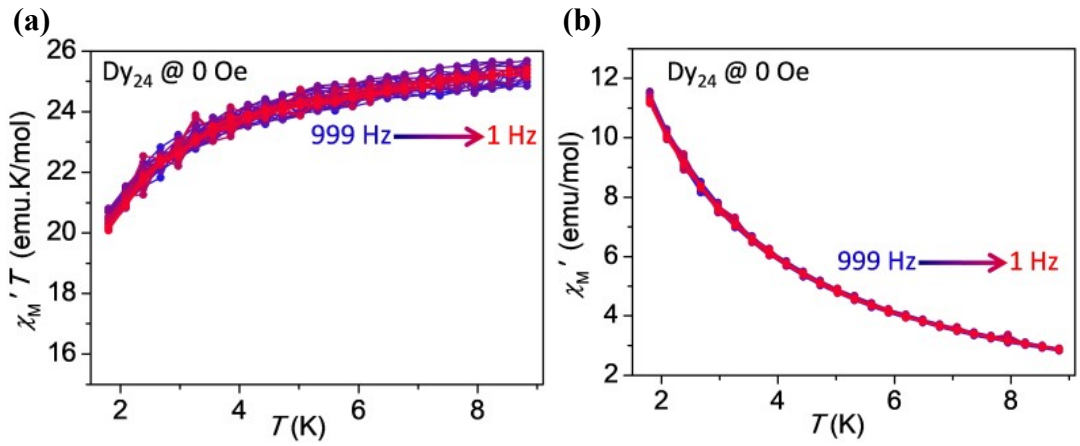

Figure S21. Temperature dependence of the $\chi_M'T$ (a) and χ_M' (b) in zero dc field for **Dy$_{24}$**.

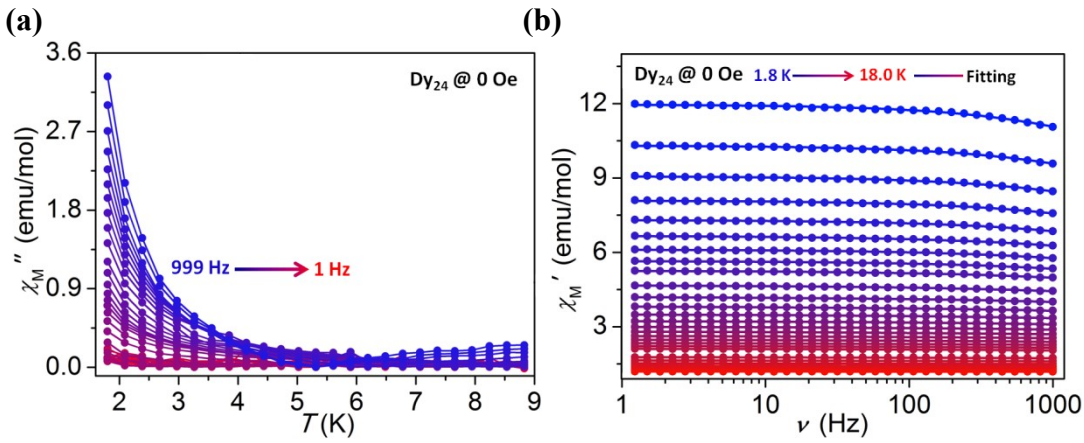

Figure S22. Temperature dependence of χ_M'' (a) and frequency dependence of χ_M' (b) in a 800 Oe dc field for **Dy$_{24}$**.

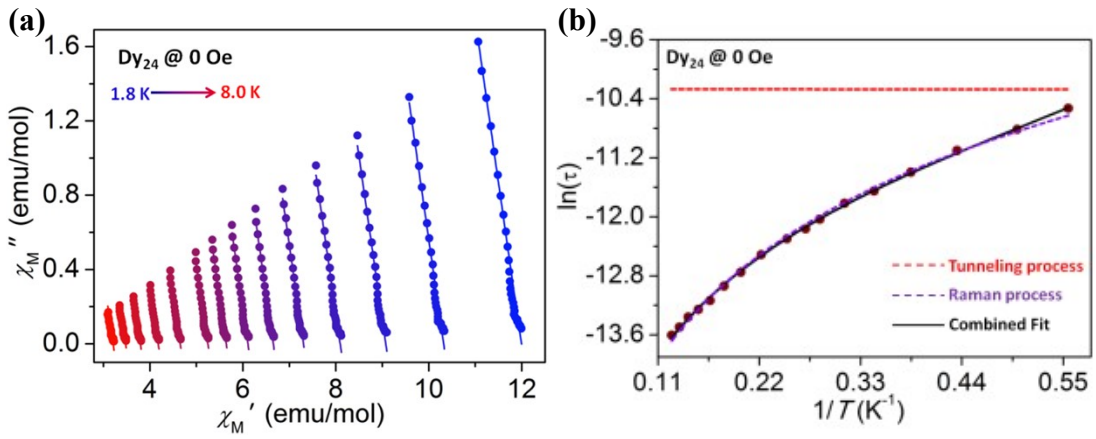

Figure S23. Cole-Cole plots for compound **Dy$_{24}$** collected under zero applied dc magnetic field. Data were collected at the temperature of 1.8 K and 8.0 K (a). The solid lines represent fits to the data using the generalized Debye model. Plots of ln(τ) *vs.* 1/T: magnetization relaxation times extracted from ac susceptibility measurements (b). Black lines represent overall fits to the data. Red and violet lines represent the quantum tunneling and Raman components of the fit, respectively.

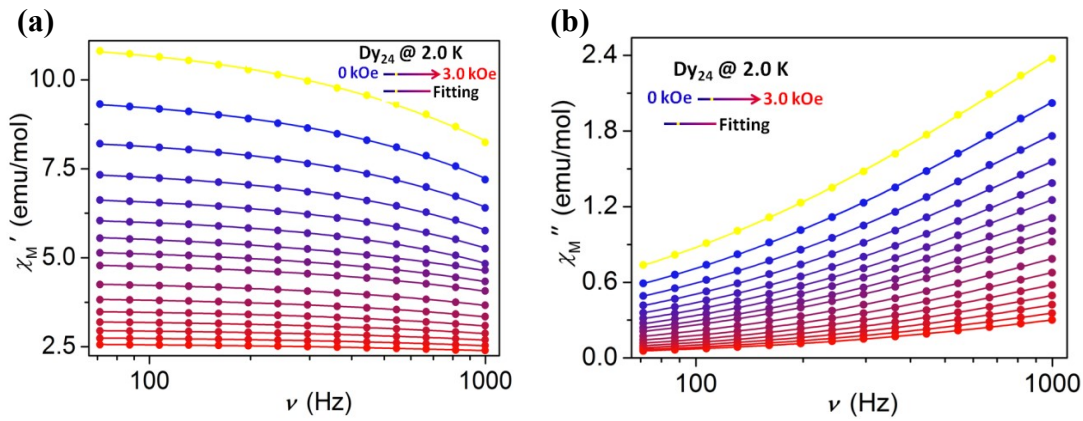

Figure S24. Frequency and field dependence of χ_M' (a) and χ_M'' (b) at 2.0 K for **Dy$_{24}$**. The solid lines are the best fits to the experimental data, obtained with the generalized Debye model.

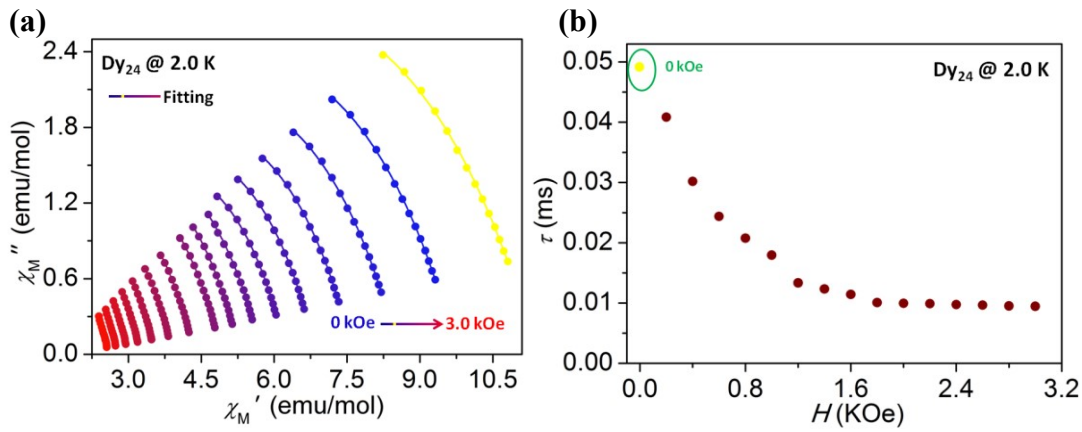

Figure S25. Cole-Cole plots at 2.0 K between 0 and 3.0 kOe for **Dy$_{24}$** (a). The solid lines are the best fits to the experiments with the generalized Debye model. Magnetization relaxation time, τ *versus* H plots (b).

Table S5. Magnetization relaxation fitting parameters from least-squares fitting of $\chi(\omega)$ data for compound **Dy$_9$** under the different applied dc field.

H (Oe)	χ_T	χ_S	α	τ / s
200	12.842(1)	12.693(1)	0.142(5)	3.306(5)E-4
400	12.504(6)	11.197(8)	0.189(7)	3.658(1)E-4
600	12.083(1)	9.203(1)	0.199(3)	4.088(1)E-4
800	11.543(1)	7.754(4)	0.236(7)	4.197(3)E-4
1000	11.006(2)	6.585(7)	0.284(2)	4.079(8)E-4
1200	10.358(5)	5.951(6)	0.285(1)	3.936(4)E-4
1400	9.757(1)	5.236(4)	0.295(9)	3.832(9)E-4
1600	9.129(5)	4.802(7)	0.308(3)	3.693(4)E-4
1800	8.703(4)	4.310(6)	0.327(6)	3.574(3)E-4
2000	7.942(1)	4.200(8)	0.332(5)	3.469(6)E-4
2200	7.333(6)	4.104(8)	0.347(7)	3.365(2)E-4
2400	6.691(4)	3.988(8)	0.381(3)	3.291(6)E-4
2600	6.701(6)	3.270(2)	0.383(2)	3.204(1)E-4
2800	6.197(2)	3.261(8)	0.418(4)	3.135(9)E-4
3000	5.387(6)	3.752(8)	0.445(6)	3.032(8)E-4

Table S6. Magnetization relaxation fitting parameters from least-squares fitting of $\chi(\omega)$ data for compound **Dy$_9$** under the optimal 800 Oe dc field.

T (K)	χ_T	χ_S	α	τ / s
1.8	30.052(6)	9.955(3)	0.326(2)	1.828(7)E-4
2.0	20.879(9)	10.988(5)	0.328(5)	1.735(4)E-4
2.3	18.011(4)	11.120(1)	0.362(1)	1.632(6)E-4
2.6	17.044(6)	12.130(3)	0.367(7)	1.564(4)E-4
2.9	15.964(7)	13.250(2)	0.371(3)	1.494(8)E-4
3.2	15.708(1)	13.241(4)	0.377(1)	1.429(9)E-4
3.5	15.236(4)	13.187(5)	0.382(6)	1.401(6)E-4
3.7	15.105(6)	13.082(2)	0.390(1)	1.400(7)E-4
4.0	14.816(3)	12.979(3)	0.427(9)	1.367(3)E-4
4.5	14.487(4)	12.860(6)	0.443(5)	1.343(1)E-4
5.0	14.250(5)	12.749(4)	0.476(7)	1.303(4)E-4
5.5	14.139(3)	12.512(5)	0.486(8)	1.276(1)E-4
6.0	14.020(6)	12.183(6)	0.495(2)	1.250(2)E-4
6.5	13.917(7)	11.895(1)	0.543(9)	1.225(1)E-4
7.0	13.812(4)	11.763(5)	0.559(6)	1.201(9)E-4
7.5	13.758(5)	11.291(8)	0.603(5)	1.183(1)E-4
8.0	13.749(7)	11.035(2)	0.622(4)	1.165(8)E-4

Table S7. Results obtained from the fitting of the frequency-dependent *ac* susceptibility for compound **Dy_9** under the optimal 800 Oe dc field.

Dy_9			
Magnetic relaxation pathway	***C*** **($s^{-1}K^{-n}$)**	***n***	***A*** **($s^{-1}K^{-1}$)**
Raman process	0.06	2.83	-
Direct process	-	-	6.48×10^{-3}
Raman and direct processes	0.13	4.69	1.54×10^{-4}

Table S8. Magnetization relaxation fitting parameters from least-squares fitting of $\chi(\omega)$ data for compound **Dy_{24}** under the different applied dc field.

H (Oe)	χ_T	χ_S	α	τ / s
0	11.202(4)	6.754(1)	0.273(7)	4.909(1)E-5
200	9.647(7)	5.833(1)	0.281(4)	4.083(9)E-5
400	8.479(6)	4.743(8)	0.293(2)	3.017(3)E-5
600	7.556(5)	3.300(1)	0.302(6)	2.437(3)E-5
800	6.812(6)	2.610(1)	0.303(5)	2.076(1)E-5
1000	6.206(6)	2.279(3)	0.310(1)	1.794(8)E-5
1200	5.814(1)	2.172(1)	0.337(1)	1.333(6)E-5
1400	5.309(6)	1.727(1)	0.343(2)	1.232(8)E-5
1600	4.930(9)	1.582(5)	0.344(3)	1.141(1)E-5
1800	4.369(7)	1.390(1)	0.348(2)	1.006(9)E-5
2000	3.922(7)	1.286(8)	0.352(1)	9.936(6)E-6
2200	3.563(1)	1.132(1)	0.355(4)	9.886(2)E-6
2400	3.261(6)	0.800(4)	0.367(3)	9.745(3)E-6
2600	3.009(2)	0.771(7)	0.390(2)	9.637(6)E-6
2800	2.795(1)	0.276(7)	0.406(1)	9.511(4)E-6
3000	2.607(9)	0.267(8)	0.415(3)	9.437(1)E-6

Table S9. Magnetization relaxation fitting parameters from least-squares fitting of $\chi(\omega)$ data for compound **Dy_{24}** under zero dc field.

T (K)	χ_T	χ_S	α	τ / s
1.8	11.963(6)	6.532(1)	0.396(2)	2.672(1)E-5
2.0	10.310(1)	6.342(6)	0.419(1)	2.007(8)E-5
2.3	9.076(9)	5.466(5)	0.454(1)	1.505(2)E-5
2.6	8.092(5)	4.532(3)	0.443(6)	1.123(7)E-5
2.9	7.308(1)	2.966(8)	0.469(4)	8.718(5)E-6
3.2	6.670(1)	2.281(8)	0.5.34(6)	7.359(7)E-6
3.5	6.118(4)	0.802(2)	0.518(8)	5.937(7)E-6
3.7	5.656(9)	0.516(8)	0.538(9)	5.209(4)E-6
4.0	5.263(3)	0.300(7)	0.563(8)	4.560(3)E-6
4.5	4.674(2)	0.561(1)	0.594(9)	3.675(6)E-6
5.0	4.209(1)	1.136(2)	0.649(4)	2.894(6)E-6
5.5	3.829(6)	1.314(8)	0.686(9)	2.400(4)E-6
6.0	3.508(7)	1.057(1)	0.683(8)	1.968(6)E-6
6.5	3.235(5)	0.829(9)	0.670(7)	1.746(5)E-6
7.0	3.018(7)	1.270(8)	0.729(6)	1.576(9)E-6
7.5	2.825(9)	1.436(1)	0.753(6)	1.374(3)E-6
8.0	2.639(4)	1.210(2)	0.716(8)	1.231(5)E-6

Table S10. Results obtained from the fitting of the frequency-dependent *ac* susceptibility for compound **Dy_{24}** under zero applied dc field.

Dy_{24}			
Magnetic relaxation pathway	***C*** **($s^{-1}K^{-n}$)**	***n***	**τ_{tunnel} (s)**
Raman process	1.19	3.04	-
Quantum tunneling process	-	-	0.006
Raman and quantum tunneling processes	1.45	6.18	0.04

REFERENCES

S1 I. P. Beletskaya, M. A. Kazankova, Catalytic Methods for Building up Phosphorus-Carbon Bond, *Russian J. Org. Chem.*, **2002**, 38, 1391-1430.

S2 Boudreaux, L. N. M. E. A., Theory and Applications of Molecular Paramagnetism, John Wiley & Sons, New York, **1976**.

S3 Rigaku Oxford Diffraction. CrysAlis^{Pro} Software system. version 1.171.42.89a, Rigaku Corporation: Oxford, UK, **2023**.

S4 L. Palatinus and G. Chapuis, SUPERFLIP - A Computer Program for the Solution of Crystal Structures by Charge Flipping in Arbitrary Dimensions, *J. Appl. Crystallogr.* **2007**, 40, 786-790.

S5 G. M. Sheldrick, Crystal structure refinement with SHELXL, *Acta Crystallogr. Sect. C.* **2015**, 71, 3–8.

S6 O. V. Dolomanov, L. J. Bourhis, R. J. Gildea, J. A. K. Howard and H. Puschmann, *OLEX2*: A Complete Structure Solution, Refinement and Analysis Program, *J. Appl. Crystallogr.* **2009**, 42, 339-341.

S7 A. L. Spek, Structure Validation in Chemical Crystallography, *Acta Crystallogr., D: Biol. Crystallogr.* **2009**, 65, 148-155.

S8 A. L. Spek, PLATON SQUEEZE: A Tool for the Calculation of the Disordered Solvent Contribution to the Calculated Structure Factors, *Acta Crystallogr., Sect. C: Struct. Chem.* **2015**, 71, 9-18.